Coupling of the solar wind to temporal fluctuations in ground magnetic fields

R. S. Weigel
NRC at NASA/GSFC, Greenbelt, MD, USA

D. Vassiliadis
USRA at NASA/GSFC, Greenbelt, MD, USA

A. J. Klimas
NASA/GSFC, Greenbelt, MD, USA

Received 16 January 2002; revised 7 March 2002; accepted 12 March 2002; published 8 October 2002.

[1] A study of the coupling of the solar wind to temporal fluctuations in high–latitude ground magnetic fields is presented. The fluctuation measure considered is the absolute value of the north-south horizontal field time derivative ($|dB_x/dt|$) averaged over a 30–minute interval. The fluctuation level is predicted using a nonlinear mapping of solar wind plasma and field measurements. The predictability of ground magnetic field fluctuations is shown to depend on both local time and latitude. For lower polar cap magnetometer locations, the coupling is highest at the local times that have the highest average fluctuation level and lowest at the local times that have the lowest average fluctuation level. The highest level of coupling is at auroral-zone latitudes in the post-midnight sector. The relative influence of different solar wind inputs is shown to be highly dependent on spatial location. *INDEX TERMS:* 2435 Ionosphere: Ionospheric disturbances; 2784 Magnetospheric Physics: Solar wind/magnetosphere interactions; 2437 Ionosphere: Ionospheric dynamics; 2447 Ionosphere: Modeling and forecasting. **Citation:** Weigle, R. S., D. Vassiliadis, and A. J. Klimas, Coupling of the solar wind to temporal fluctuations in ground magnetic fields, *Geophys. Res. Lett.*, *29*(19), 1915, doi:10.1029/2002GL014740, 2002.

1. Introduction

[2] The amplitude of composite auroral electrojet disturbance indices such as *AL*, *AU*, and *AE* have been shown to be predictable by using information measured in the upstream solar wind. On time scales of one minute, approximately 40%–70% of the variance in the amplitude of these indices can be predicted from solar wind data alone [*Clauer*, 1986; *Hernandez et al.*, 1993; *Vassiliadis et al.*, 1995; *Gleisner and Lundstedt*, 1997]. Although these results indicate that much of the variance in these indices can be explained by the solar wind, they are difficult to use for the prediction of geomagnetically induced currents (GICs). The indices are computed from magnetometer traces from different spatial locations and prediction algorithms tend to miss rapid jumps in amplitude, as noted by *Gleisner and Lundstedt* [1997] and *Gavrishchaka and Ganguli* [2001]. GICs are correlated with the amplitude of auroral electrojet indices, but they are physically related to the time derivative of the ground magnetic field [*Pirjola*, 2000]. Given the amplitude of temporal magnetic fluctuations and the local ground conductivity, the induced electric fields responsible for GICs can be estimated directly [*Pirjola and Viljanen*, 1998; *Boteler and Pirjola*, 1998].

[3] Although much is known about how the solar wind couples to the amplitude of geomagnetic disturbances, comparatively little is known about the coupling of the solar wind to the time rate of change of geomagnetic disturbances. As shown by *Viljanen* [1997], the average amplitude of $|dB/dt|$ depends on both local time and latitude. Here we show that the coupling of the solar wind to $|dB_x/dt|$ also has a sensitive dependence on local time and latitude. This coupling is demonstrated through the use of nonlinear coupling functions that map solar wind data to $|dB_x/dt|$.

[4] The optimal coupling function between the solar wind and the fluctuation amplitude $|dB_x/dt|$ is found by a direct mapping of solar wind data. The fluctuation amplitude is predicted directly, in contrast to an algorithm that uses a prediction of B_x to compute $|dB_x/dt|$. The measure of fluctuation considered is the average of $|dB_x/dt|$ in a 30–minute interval. This averaging interval is small enough to give an approximately 30–minute prediction lead time for a satellite 60 minutes upstream of Earth, and is long enough to allow for computations to be performed on a two-year data set.

[5] In addition to revealing the nature of SW–$|dB_x/dt|$ coupling, these results are important for assessing the risk of GICs. For example, although some locations have a comparatively high average amplitude of $|dB_x/dt|$, their amplitude may be more easily predicted if they are closely coupled to the solar wind. Conversely, some locations that have a low average amplitude of $|dB_x/dt|$ may be effectively unpredictable from a time history of the solar wind state.

2. Method

[6] The data used in this study consists of ground magnetometer measurements at one-minute resolution for days 23–365 of 1998 and all days of 1999 from the IMAGE stations NAL, LYR, HOR, HOP, BJN, SOR, ABK, KIR, SOD, OUJ, HAN, NUR [*Luhr et al.*, 1998]. The solar wind magnetic field data is from the ACE satellite located

0094-8276/02/2002GL014740$05.00

approximately 60 minutes upstream of Earth. The solar wind magnetic field data (in GSM coordinates) was interpolated from 16 second averages to a one–minute time grid. The solar wind ion velocity (in GSM) data was interpolated from 64 second averages to a one–minute time grid.

[7] The fluctuation amplitude D at a magnetometer m is the block average with window width t_a = 30 minutes

$$D_t^m = \frac{1}{t_a} \sum_{j=t-\frac{t_a}{2}}^{t+\frac{t_a}{2}-1} \left| \frac{\Delta B_{x(j)}}{\Delta t} \right|, \tag{1}$$

where $\Delta t = t_j - t_{j-1} = 1$ minute and $\Delta B_x = B_{x(t)} - B_{x(t-1)}$. The prediction lead time is $t_d - 30$ minutes, where t_d is the time it takes the solar wind to travel from ACE to the magnetopause (the time of communication from the satellite to Earth is small and is ignored). Because the solar wind speed is variable, the prediction lead time is also variable. The average delay time for this data set is 62 minutes and the minimum is 30 minutes.

[8] To determine the coupling of the solar wind to the disturbance level, a mapping based on an input vector containing only solar wind data is used. A different mapping function is generated for each of the 48 possible local times and for each magnetometer station, m. The predicted disturbance $\mathcal{D}$ in the interval centered at time t is approximated by a nonlinear mapping of two hours of time delayed solar wind information

$$\mathcal{D}_t^m = f_{LT}^m([\mathbf{I}_{t-t_d}, \mathbf{I}_{t-t_d-t_a}, \mathbf{I}_{t-t_d-2t_a}, \mathbf{I}_{t-t_d-3t_a}]), \tag{2}$$

where the parameters of the mapping function f are determined by minimizing the error between the measured disturbance D and the predicted disturbance $\mathcal{D}$ using the days of the training set.

[9] The solar wind inputs are the measured variables

$$\mathbf{I}_t = [\rho_i, B_z, v_x], \tag{3}$$

and not a predetermined coupling function. This method allows the network to determine the appropriate coupling function so that the coupling function is data-derived. All of the input quantities have been averaged over an interval of t_a centered on time t.

[10] The measure of coupling or predictability is the prediction efficiency [*Detman and Vassiliadis*, 1997],

$$PE_{LT}^m = 1 - \frac{E_{LT}^m}{\sigma_D^2}, \tag{4}$$

where the error at magnetometer m is

$$E_{LT}^m = \left\langle \left(D_t^m - \mathcal{D}_t^m\right)^2 \right\rangle_{LT}, \tag{5}$$

and $\langle \cdot \rangle_{LT}$ indicates an average over all intervals that are centered on local time LT. The prediction error for a magnetometer at each of the 48 local times is determined by averaging over the common local times from the days of the test set. The PE is the fraction of the variance in D at local time LT that is predicted by $\mathcal{D}$. A prediction efficiency of zero means that the prediction is as good as a prediction that uses only the average value as a predictor. If the mean and standard deviation of the predicted and measured value are equal, and the prediction error is uncorrelated with the prediction, PE is identical to the square of the correlation coefficient R^2. Here we use the PE notation to emphasize that these are out-of-sample correlations.

[11] To eliminate any bias due to the choice of days used for the training and test sets, a random sample of half of the days of the data set was used for the training set; the remaining days were used as the test set. All PE values reported are averages of the test set error for 100 different random choices of training and test sets. This method serves to eliminate any bias that would occur if, for example, an exceptional number of days of the training set were quiet days while the test set contained mostly disturbed days. Also, any seasonal dependence is removed, although ideally the mapping function would be dependent on season and year [*Viljanen et al.*, 2001], especially for the higher latitude locations. For this analysis, the PEs can be interpreted as showing how much of the disturbance at a given magnetometer can be derived from the solar wind using an out-of-sample data set.

[12] We use a neural network as the nonlinear mapping function since it can approximate almost any continuous input/output mapping [*Hertz et al.*, 1991]. The mapping function f for each magnetometer is a neural network in the form of a multi–layer perceptron [*Bishop*, 1995]

$$f(\mathbf{I}) = \sum_{i=1}^{M} W_i \sum_{j=1}^{N} \tanh\left(w_{ij} I_j + a_i\right) + A. \tag{6}$$

In the limit of $w_{ij} I_j + a_i \ll 1$ for all ij, the mapping is a linear moving average filter similar to that used in models which predict the amplitude of the ground magnetic field, **B**. The $M(N + 2) + 1$ weights are determined using the scaled conjugate gradient descent minimization method with the input–output vectors of the training set. The number of weights of the input layer N is fixed by the dimension of the input vector.

3. Results

[13] In Figure 1 the averages of $|dB_x/dt|$ are shown. These averages were generated by computing the 30-minute average of $|dB_x/dt|$ for each magnetometer for all days of the data set. There are two peaks in the surface. The largest is located in the pre–midnight sector. This location corresponds to the transition region from the maximum eastward electrojet, corresponding to large positive B_x, to the maximum westward electrojet, corresponding to large negative B_x. The second peak, located in the pre-noon sector, can also be explained as a transition region from westward to eastward electrojets. The first peak extends to lower latitudes as would be expected from the expansion of the auroral oval in the midnight sector during substorms and highly active times. In terms of physical processes, the pre-midnight peak is primarily a result of substorm activity, and the pre-noon sector is primarily a result of ULF pulsations.

[14] Figure 1 contains only one component of the ground magnetic field. Generally dB_x/dt alone is a sufficient proxy

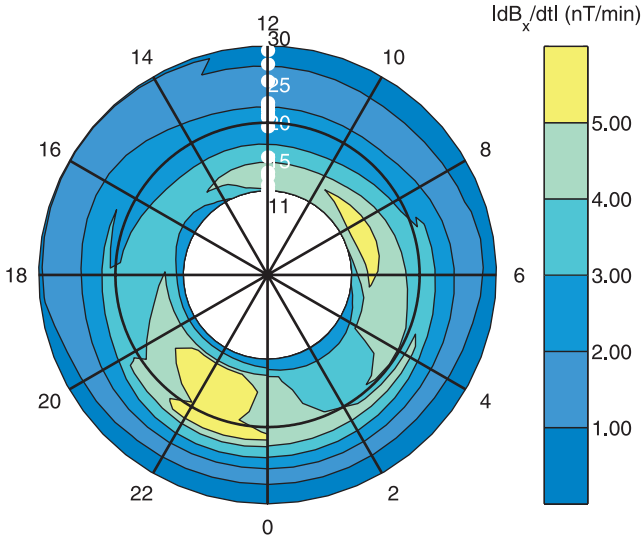

Figure 1. Average value of $|dB_x/dt|$ for the stations listed in Table 1 as a function of local time and geographic latitude. Dots on the LT = 1200 axis indicate the geographic latitude of the magnetometer stations.

for the local and temporal behavior of the average level of dB/dt [*Boteler et al.*, 1998; *Vennerstrøm*, 1999; *Viljanen et al.*, 2001]. *Gleisner and Lundstedt* [2001] have shown that there is a difference between the predictions of the horizontal amplitudes for the B_x and B_y directions. Therefore, we should also expect a difference between the *PE* surfaces of $|dB_x/dt|$ and $|dB_y/dt|$. Here we chosen to focus on only the north–south component because it is more closely connected to changes in the auroral electrojets.

[15] In Figure 2 the level of coupling of $|dB_x/dt|$ to the solar wind, in terms of the *PE* of the model, is shown. In general, the *PE* is highest in the auroral–zone and has a slight minimum in the pre-dusk sector. The location of maximum *PE* occurs in the post–midnight sector; this location is also where the nonlinear model outperforms

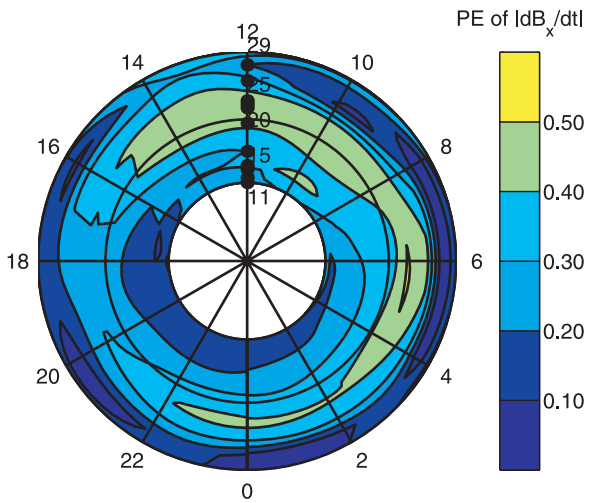

Figure 2. Prediction efficiency of the nonlinear model that predicts the 30–minute average of $|dB_x/dt|$ given two hours of solar wind data. The error (uncertainty) surface is approximately ±0.05.

the linear model by the greatest margin, and is the location where the solar wind magnetic field B_z has the greatest influence on the model (discussed below). For the higher latitude stations, the *PE* surface tends to follow the average $|dB_x/dt|$ surface, with higher amplitudes of the *PE* occurring where the average of $|dB_x/dt|$ is the highest. This is not the case for the auroral–zone latitudes where the *PE* is roughly constant for most local times, while the average level of $|dB_x/dt|$ varies from 3–6 nT/min.

[16] Because we have determined the optimal input function from the data, we can consider the relative importance of the solar wind inputs as a function of geographic location. This is done by determining the optimal network using the individual components of the solar wind input vector of Equation 3. Figure 3 compares the relative performance of a coupling function that uses only $\mathbf{I} = v_x$ to one that uses only $\mathbf{I} = B_z$. In addition, the composite curve derived using $\mathbf{I} = [v_x, B_z]$ is shown. For the high–latitude station NAL, v_x is the most important driver of $|dB_x/dt|$, while the solar wind magnetic field B_z has a very small contribution. This result reveals the importance of allowing for a data–derived coupling function: if $\mathbf{I} = v_x B_s$ is used, its *PE* curve will be zero in the locations where the $PE(B_z)$ curve is zero, since B_z is essentially a random variable at these locations.

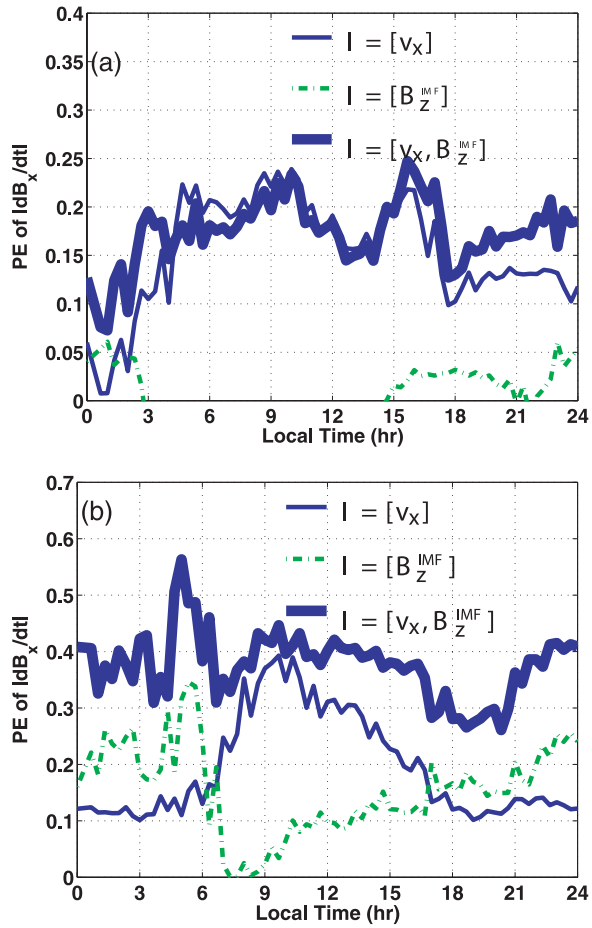

Figure 3. Comparison of relative contribution to *PE* of solar wind v_x and B_z for (a) lower polar cap magnetometer NAL and (b) auroral–zone latitude magnetometer SOD.

[17] For the auroral-zone station SOD, the average levels of *PE* are higher. Figure 3b shows that a substantial part of the activity at auroral latitudes can be derived from the solar wind magnetic field B_z, especially in the post–midnight region. The solar wind velocity has the highest influence at approximately dawn. The maximum value of the $PE(v_x)$ curve of 0.4 is consistent with *Vennerstrøm* [1999] who found that the (in-sample) R^2 between v_x and the log of the power spectral density of H in the 2–4 and 5–10 minute band was approximately 0.5 for high-latitude magnetometers in the morning sector. The range of *PE* values for the SW–$|dB_x/dt|$ mapping measurements is comparable to that found by *Gleisner and Lundstedt* [2001] for SW–B_x mappings. However, the local time variation is quite different, since the SW–B_x mapping has peaks centered at noon and midnight.

[18] The local time asymmetry about noon for the $PE(v_x)$ curve is similar to that observed in Pc5 index amplitudes at auroral latitudes [*Engebretson et al.*, 1998]. This asymmetry has been attributed to typical IMF configurations that give a higher probability of the Kelvin-Helmholtz instability criteria being satisfied in the pre-noon sector [*Lee and Olson*, 1980].

[19] The role of the ion density, ρ_i in driving $|dB_x/dt|$ is small. In general, the *PE* of a model that uses ρ_i is zero (within error), indicating that the ion density (statistically) contains no information that explains the dynamics of $|dB_x/dt|$.

4. Conclusions

[20] By directly mapping solar wind measurements to the ground magnetic field fluctuation level we have shown that their coupling is highly variable and dependent on geographic location. The average relative influence of the solar wind as a function of spatial location was determined by deriving a global map of the *PE* of a model that predicts $|dB_x/dt|$ given solar wind data. The global map of *PE* shows that although some locations have comparatively low average values of $|dB_x/dt|$, they may be more dangerous in a space weather sense since they are are not strongly coupled to the solar wind (or well predicted given solar wind data).

[21] By determining the optimal coupling function from the data, we have shown that no single solar wind input coupling function (e.g. v_xB_s, $v_x^2B_s$, etc.) is appropriate for all spatial locations. For high–latitude stations, the solar wind velocity is highly coupled to $|dB_x/dt|$, while the IMF magnetic field B_z has very little influence, on average. At auroral–zone latitudes, the IMF magnetic field has the most influence in the post–midnight sector, while the solar wind velocity has the most influence in the dayside sector.

[22] Since the angle between geomagnetic north and geographic north is small at the locations of the IMAGE magnetometer chain, $|dB_x/dt|$ is a measure of the time rate of change in the eastward and westward flowing (equivalent) ionospheric currents. Ideally, all three components of the field would be predicted, since the contribution of dB_y/dt and dB_z/dt to the total induced electric field can be large [*Viljanen*, 1997]. Although the time rate of change of the ground magnetic field is a proxy for the geomagnetically induced currents, we have shown that both the amplitude and coupling to the solar wind are important for assessing risk. That is, locations that are highly coupled to the solar wind may have less GIC risk than locations that have the same average value of $|dB/dt|$, but are not coupled to the solar wind. The emphasis here has been on how the solar wind couples to fluctuations in the ground magnetic field (in terms of the prediction error). For the estimation of risk, methods that employ decision theory [*Thomson*, 2000] or that use a prediction which minimizes a risk measure [*Gavrishchaka and Ganguli*, 2001] are more appropriate than the models that only minimize the prediction error.

[23] **Acknowledgments.** We thank the institutes that maintain the IMAGE magnetometer array and the PI institute for IMAGE: the Finnish Meteorological Institute (www.geo.fmi.fi/image).

References

Bishop, C. M., Neural networks for pattern recognition, Oxford University Press, 1995.

Boteler, D. H., and R. J. Pirjola, The complex-image method for calculating the magnetic and electric fields produced at the surface of the Earth by the auroral electrojet, *Geophysical J. Int.*, *132*(1), 31–40, 1998.

Boteler, D. H., R. J. Pirjola, and H. Nevanlinna, The effects of geomagnetic disturbances on electrical systems at the Earth's surface, *Adv. Space Res.*, *22*, 17–27, 1998.

Clauer, R. C., The technique of linear prediction filters applied to studies of solar wind–magnetosphere coupling, Solar Wind–Magnetosphere Coupling, edited by Y. Kamide and J. A. Slavin, 39–57, 1986.

Detman, T., and D. Vassiliadis, Review of Techniques for Magnetic Storm Forecasting, in Magnetic Storms, *Geophysical Monograph*, 98, American Geophysical Union, 1997.

Engebretson, M., K.-H. Glassmeier, and M. Stellmacher, The dependence of high-latitude Pc5 wave power on solar wind velocity and on the phase of high-speed solar wind streams, *J. Geophys. Res.*, *103*(A11), 26,271, 1998.

Gavrishchaka, V. V., and S. B. Ganguli, Optimization of the neural-network geomagnetic model for forecasting large-amplitude substorm events, *Journal of Geophysical Research-Space Physics*, *106*(A4), 6247–6257, 2001.

Gleisner, H., and H. Lundstedt, Response of the auroral electrojets to the solar wind modeled with neural networks, *J. Geophys. Res.*, *102*(A7), 14,269, 1997.

Gleisner, H., and H. Lundstedt, A neural network-based local model for prediction of geomagnetic disturbances, *J. Geophys. Res.*, *106*(A5), 8425–8433, 2001.

Hernandez, J. V., T. Tajima, and W. Horton, Neural net forecasting for geomagnetic activity, *Geophys. Res. Lett.*, *20*, 2707, 1993.

Hertz, J., A. Krogh, and R. G. Palmer, Introduction to the theory of neural computation, Addison–Wesley Publishing Company, 1991.

Luhr, H., A. Aylward, S. C. Bucher, A. Pajunpaa, K. Pajunpaa, T. Holmboe, and S. M. Zalewski, Westward moving dynamic substorm features observed with the IMAGE magnetometer network and other ground-based instruments, *Annales Geophysicae-Atmospheres Hydrospheres and Space Sciences*, *16*(4), 425–440, 1998.

Pirjola, R., Geomagnetically induced currents during magnetic storms, *IEEE Trans. on Plasma Science*, *28*(6), 1867–1873, 2000.

Pirjola, R., and A. Viljanen, Complex image method for calculating electric and magnetic fields produced by an auroral electrojet of finite length, *Annales Geophysicae*, *16*, 1434–1444, 1998.

Pirjola, R., D. Boteler, A. Viljanen, and O. Amm, Prediction of geomagnetically induced currents in power transmission systems, *Advances in Space Research*, *26*, 5–14, 2000.

Thomson, A. W. P., Evaluating space weather forecasts of geomagnetic activity from a user perspective, *Geophys. Res. Lett.*, *24*(24), 4049, 2000.

Vassiliadis, D., A. J. Klimas, D. N. Baker, and D. A. Roberts, A Description of the Solar-Wind Magnetosphere Coupling Based On Nonlinear Filters, *J. Geophys. Res.*, *100*(A3), 3495–3512, 1995.

Vennerstrøm, S., Dayside magnetic ULF power at high latitudes: A possible long-term proxy for the solar wind velocity?, *J. Geophys. Res.*, *104*, 10,145, 1999.

Viljanen, A., The relation between geomagnetic variations and their time derivatives and implications for estimation of induction risks, *Geophys. Res. Lett.*, *24*(6), 631, 1997.

Viljanen, A., H. Nevanlinna, K. Pajunpaa, and A. Pulkkinen, Time derivative of the horizontal geomagnetic field as an activity indicator, *Ann. Geophys.*, *19*, 1107, 2001.

Wu, J. G., and H. Lundstedt, Neural network modeling of solar wind magnetosphere interaction, *J. Geophys. Res.*, *102*(A7), 14,457–14,466, 1997.

R. S. Weigel, NRC at NASA/GSFC, Greenbelt, MD 20771, USA.
D. Vassiliadis, USRA at NASA/GSFC, Greenbelt, MD 20771, USA.
A. J. Klimas, NASA/GSFC, Greenbelt, MD 20771, USA.